Effects of pulsed hollow electron lens operation on the beam core in HL-LHC: First experimental studies and simulations.*

Miriam Fitterer,[†] Giulio Stancari, and Alexander Valishev
Fermi National Accelerator Laboratory, Batavia, Illinois, USA

Giulia Papotti, Stefano Redaelli, and Daniel Valuch
CERN, Geneva, Switzerland
(Dated: December 26, 2017)

In the HL-LHC a considerable amount of energy is stored in the beam tails due to the high beam intensity and an overpopulation of the tails compared to a Gaussian distribution. To control and clean the tail population, the installation of two hollow electron lenses, one per beam, is considered. Beside the DC operation, also a pulsed operation of the hollow electron lens is considered, which would considerably increase the diffusion speed by putting noise on the halo particles. In the ideal case, that is in case of no field at the beam core, only the halo particles are excited while leaving the core unperturbed. The picture though changes, if a residual field is present also at the location of the beam core putting noise also on the beam core. In this paper we present for estimates of the residual field at the beam core expected from the HL-LHC hollow electron lens and first experimental results of the effect of this excitation on the beam core together with the supporting simulations.

I. INTRODUCTION

Considering past, current and future high energy and intensity colliders, each new machine has represented a considerable leap in stored beam energy with rising values for future accelerators and colliders (see Table I). Recent measurements at the LHC furthermore show that the tails of the transverse beam distribution are overpopulated compared to a Gaussian distribution resulting in a considerable amount of energy being stored in the beam tails alone. In case of the LHC explicitly around 5% of the beam population is stored in the tails above 3.5 σ compared to 0.22% in case of a Gaussian distribution leading to 19 MJ of stored energy in the tails in case of nominal LHC parameters and 34 MJ in case of HL-LHC [6].

All of the above reasons lead to the conclusion that a mechanism is needed to deplete the beam tails in a controlled manner (see for example [7] in case of HL-LHC). The most obvious idea is to decrease the collimator gaps or scrape the tails with a collimator type device. The minimum gap size of the collimators is however limited by the impedance of the machine and small enough gap sizes can therefore not be reached without risking an instability of the beam. Other mechanisms must therefore be found to actively deplete the tails.

Most promising are methods, which considerably increase the diffusion speed in the region of the halo particles while leaving the beam core unperturbed. The diffus-

ing halo particles are then intercepted by the collimation system and removed (see Fig. 1 for illustration). This concept is also referred to as active halo control compared to a passive system, which only intercepts the halo particles without actively controlling the diffusion speed. Currently, the LHC collimation system is a passive halo control system.
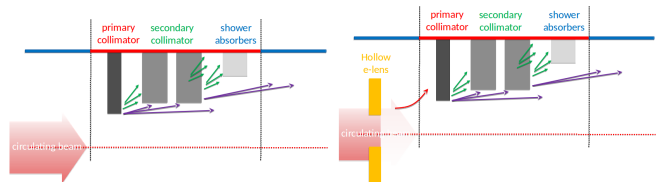

FIG. 1. Sketch of passive halo control as with the collimation system (top) and active halo control using in addition for example a hollow electron lens (HEL) to control the diffusion speed in the region tail region without affected the beam core (bottom). Any acknowledgement needed for the plots?.

In view of the need of an active halo control system for LHC and HL-LHC in particular and in general for future high power accelerators, different methods have been studied in the last recent years [8], of which the HEL is considered the superior device at least in case of the HL-LHC [7] and is also considered for other future high energy colliders like HE-LHC and FCC-hh [9?].

The beneficial effect of an active halo control system is however abrogated if also the beam core is affected as this would ultimately lead to a degradation of the performance due to losses of particles in the core region and emittance growth. In this paper, we will concentrate on this aspect in view of future HEL to be installed in the HL-LHC. We will summarize possible sources of perturbations of the beam core concentrating in particular on the case of pulsed operation and with the focus on the beam experiments at the LHC performed in this context.

TABLE I. Stored beam energy for different past, present and future colliders. Each new machine represents a leap in stored beam energy.

Collider	Tevatron (protons) [1]	LHC 2016 [2]	LHC nominal [3]	HL-LHC [4]	FCC [5]
Beam energy [TeV]	0.98	6.5	7.0	7.0	50.0
Number of bunches	36	2220	2808	2748	?
Number of particles per bunch	2.90×10^{11}	1.15×10^{11}	1.15×10^{11}	2.2×10^{11}	1.0×10^{11}
Stored beam energy [MJ]	1.6	265.9	362.2	678.0	8400

This paper is structured as follows: Section II gives an introduction to the concept of HELs and summarizes the design parameters of the HL-LHC HEL. Section III is dedicated to describing the sources of a residual field from the HEL in the core region. Section IV A–**??** describes then in detail the two beam experiments conducted at the LHC to study the effect on the beam core in case of a pulsed HEL operation. This includes the detailed analysis of the observed losses, emittance and transverse beam distribution changes. To the knowledge of the authors, the observed distribution changes presented in this paper have never been measured before in the context of a resonant excitation. A resonant excitation has been previously studied at the Tevatron in the context of the HEL experiments [10] and the abort gap cleaning used in operation [11]. Both studies however only concentrated on the losses and emittance changes without measuring the detailed changes of the distribution itself. In addition, the presented experiments also provide scalings of the losses and emittance growth with the excitation amplitude. This allows to provide first tolerances for the residual field of the HL-LHC HEL at the beam core and also to compare the obtained results with simulations and thus benchmark the same.

II. HOLLOW ELECTRON LENS FOR HL-LHC

A. General Overview

In general, electron lenses are DC or pulsed low energy electron beams. The electron beam is generated in an electron gun, then guided and confined by strong solenoids and finally dumped onto a collector. Exemplary for the conceptual design of all electron lenses, the HL-LHC HEL is shown in Fig. 2. The circulating beam, in
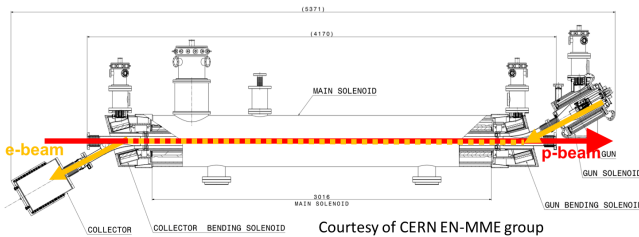

FIG. 2. Layout of HL-LHC HEL.

case of the LHC the proton beam, is then affected by the electromagnetic field of the electron beam. For the application of active halo control, the electron beam needs to generate an electromagnetic field at the location of the halo particles while leaving the core untouched. This can be achieved by using a uniform hollow distribution in radius $r = \sqrt{x^2 + y^2}$ with inner radius R_1 and outer radius R_2. In this case, the circulating proton beam experiences a radial kick $\theta(r)$

$$\theta(r) = \frac{f(r)}{(r/R_2)} \cdot \theta_{\max}, \quad (1)$$

where $f(r)$ is a shape function with

$$f(r) = \begin{cases} 0 & , \quad r < R_1, \\ \frac{r^2 - R_1^2}{R_2^2 - R_1^2} & , \quad R_1 \leq r < R_2, \\ 1 & , \quad R_2 \leq r \end{cases} \quad (2)$$

and $\theta_{\max} = \theta(R_2)$ is the maximum kick angle given by

$$\theta_{\max} = \theta(R_2) = \frac{2LI_T(1 \pm \beta_e\beta_p)}{4\pi\epsilon_0 \cdot \left(\frac{q}{p_0}\right)_p \cdot \beta_e\beta_p c^2} \cdot \frac{1}{R_2}, \quad (3)$$

where L is the length of the e-lens, I_T the total electron beam current, β_e and β_p the relativistic β of electron and proton beam, $\frac{q}{p_0} = (B\rho)_p$ the magnetic rigidity for the reference particle, c the speed of light and ϵ_0 the vacuum permittivity.

The distribution together with the resulting kick are illustrated in Fig. 3. The $\pm$-sign represents the two cases of the electron beam traveling in the direction of the proton beam ($v_e v_p > 0$) leading to "$-$" or in the opposite direction ($v_e v_p < 0$) leading to "$+$". For hollow electron beam collimation, electron and proton beam travel in opposite directions. Assuming HL-LHC and HEL design parameters (Table II–III) the maximum kick of the HEL is:

$$\theta_{\max,\mathrm{B1}} = 392 \text{ nrad} \quad (4)$$

for an inner radius $R_1 = 4\sigma_p$, outer radius $R_2 = 7.5\sigma_p$ and a peak current of $I_e = 5.0$ A. Similar values are obtained for Beam 2.

B. Operation modes and effects on the beam core

As depicted in Fig. 3 and in evidence from Eq. 1–2, the field at the beam core vanishes in the ideal case. Effects

TABLE II. HL-LHC hollow electron lens parameters as in [12].

Geometry	Value	Unit
Length L	3	m
Desired range of scraping positions[a]	4-8	σ_p
Magnetic fields		
Gun solenoid, B_g	0.2-0.4	T
Main solenoid, B_m	2-6	T
Collector solenoid, B_c	0.2-0.4	T
Compression factor ($k = \sqrt{B_m/B_g}$)	2.2-5.5	-
Electron gun		
Peak yield I_e at 10 keV	5.0	A
Gun perveance P	5	μperv
Inner/outer cathode radius, R_1/R_2	6.75/12.7	mm
High voltage modulator		
Cathode-anode voltage	10.0	kV
Rise time (10%-90%)	200	ns
Repetition rate	35	kHz

[a] σ denotes here the Beam sigma and not the collimation σ which assumes a normalized emittance of 3.5 μm.

on the beam core thus only arise in case of imperfections, where possible sources are the bends of the HEL, as the electron beam crosses directly the proton beam, and distortions in the electron beam profile (see Section III). Both sources result in non-linear kicks (see for example [13, 14] (is there a better reference for the profile imperfections, updated note from Giulio???)).

In DC operation of the HEL, the non-linear kicks from the HEL stay in the shadow of the non-linearities otherwise present in the machine. Tolerances on imperfections are therefore not particular stringent and not a concern. The picture however changes significantly in case of pulsed operation of the HEL, in which case the electron gun voltage is modulated using a white or colored noise spectrum. If the electromagnetic field of the HEL does not vanish at the proton beam core, noise is transferred not only to the halo particles, as intended, but also to
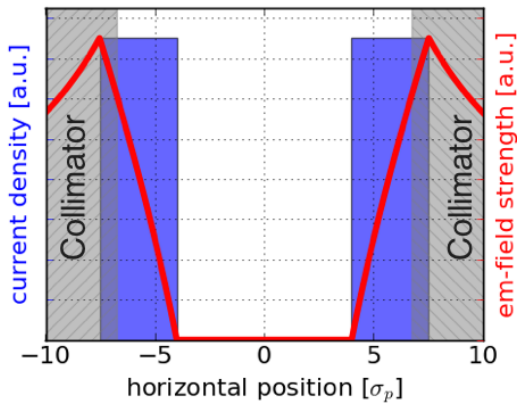

FIG. 3. Illustration of the hollow electron beam distribution (blue), the kick experienced by the proton beam (red) and the collimators (gray).

TABLE III. HL-LHC design parameters at top energy [4] and parameters relevant in connection with the HEL. Optics parameters at HEL are based on a position of the HEL of -40 m for Beam 1 (B1) and $+40$ m for Beam 2 (B2) from IP4 using HL-LHC optics V1.3 with $\beta^* = 0.15$ m [15].

Beam parameters	Value(B1)	Value(B2)	Unit
Beam energy E_p	7		TeV
Number of bunches n_b	2748		-
Number of particles per bunch N_b	2.2×10^{11}		-
Normalized emittance $\epsilon_{N,x/y}$	2.5		μm
Bunch spacing	25		ns
Optics paramters at HEL (Beam 1) [a]			
β_x at HEL	197.5	280.6	m
β_y at HEL	211.9	262.6 m	
Dispersion D_x at HEL	0.0	0.0	m
Dispersion D_y at HEL	0.0	0.0	m
Proton beam size $\sigma_{p,x}$ at HEL	0.26	0.31	mm
Proton beam size $\sigma_{p,y}$ at HEL	0.27	0.30	mm
scraping position			
$\sigma_p = \max(\sigma_{p,x}, \sigma_{p,y})$	0.27	0.31	mm

[a] As the twiss parameters at IP4 do not change during the entire squeeze, and IP4 and the HEL are only separated by a drift space, the twiss parameters stay constant also at the HEL during the entire squeeze.

the beam core with naturally much smaller amplitude. Tolerances in this case rapidly become much more stringent than in DC operation and studies of the effect of the HEL on the beam core are therefore focusing on this mode of operation.

The main benefit of pulsing the HEL is to increase the halo removal rate in case a fast depletion of the halo is desired. The halo diffusion rate is increased in this case as in addition to the non-linear kick, noise is exerted on the halo particles of the proton beam. For the HL-LHC two different pulsing patterns are currently being considered:

- **random excitation:** The electron gun voltage is modulated between:

$$U_{e-gun} = a \cdot U_{max} \qquad (5)$$
$$+(1-a) \cdot ran(0,1) \cdot U_{max} \qquad (6)$$

  with U_{max} the equivalent voltage in DC operation, a the modulation strength with $a \in [0,1]$, and $ran(0,1)$ a uniformly distributed random number between [0,1].

- **resonant excitation:** The HEL is switched on only every k^{th} turn. The excitation can then be represented by:

$$f(t) = \sum_{p=-\infty}^{+\infty} \delta(t - n \cdot (kT)), \qquad (7)$$

  where p is the turn number and T the revolution

time, and its Fourier series by:

$$f(t) = \text{III}_{kT}(t) = \frac{1}{kT} \sum_{n=-\infty}^{+\infty} e^{2\pi i f_n t} \tag{8}$$

$$\text{with } f_n = \frac{n}{k} f_{\text{rev}}, \tag{9}$$

where III_{kT} is the Dirac comb. As can be seen from the Fourier series, k^{th} turn pulsing in general drives k^{th} order resonances [16]. Historically, the kth turn pulsing was used in regular operation in the Tevatron for abort cleaning [11].

In general, the random excitation mode is the most effective and operationally easiest pulsing mode, but also the most stringent in terms of tolerances on the residual field at the beam core as it induces white noise and thus excites all beam frequencies. As the resonant excitation acts on specific resonances, the pulsing pattern has to be chosen according to the machine and beam parameters. On the one hand, this makes the operation more difficult as one has to find the most efficient k^{th} turn pulsing for each operation mode, on the other hand, it also relaxes the tolerances on the residual field at the beam core as, depending on the machine and beam configuration, it might be possible to find a resonant excitation pattern, which mainly affects the halo and not the core.

III. SOURCES OF RESIDUAL FIELD IN THE PROTON BEAM CORE REGION AND FIRST ORDER ESTIMATES

With the current HEL layout (see Fig. 2), parasitic kicks on the proton beam core can arise in the central region (main solenoid) due to profile imperfections in the electron beam and at the entrance and exit of the HEL, where electron and proton beam overlap. Currently, no HEL is installed in the LHC, and the kick on the proton beam core must therefore be approximated to first order by a dipole kick for the experiments at the LHC. Explicitly, the dipole kick with the corresponding excitation pattern is applied with the LHC transverse damper (see Section IV B).

The expected kick to first order from the HEL bends (Eqn. 14) is

$$\Delta x'_{\text{bends}}, \Delta y'_{\text{bends}} \leq 0.5 \, \text{nrad}, \tag{10}$$

and for the central region due to profile imperfections (Eqn. 15):

$$\Delta x'_{\text{central region}}, \Delta y'_{\text{central region}} \leq 15.0 \, \text{nrad} \tag{11}$$

where the current HEL design parameters (see Table III–II) are used. The contribution from the central region is clearly dominating. A more detailed derivation of both values is given in Sec. III A–III B.

A. Uncompensated kicks from HEL bends

As reference for the estimate of the dipole component originating from the HEL bends, the symplectic map derived in [13] is used. In this case the HEL bends are modeled as a cylindrical pipe with a static charge distribution of 1 A and 5 keV electrons bend in the horizontal plane. In case of an U-shaped HEL, the transverse dipole kicks at entrance and exit add up, while for a S-shaped HEL the kicks compensated each other. For this reason a S-shape has been chosen for the HL-LHC HEL (see Fig. 2). In this case, uncompensated kicks therefore only arise from imperfections, which can originate from profile imperfections and current fluctuations. As a first rough estimate, we assume in this paper 10% fluctuations between the entrance and exit and that the kicks from entrance and exit due to these imperfections add up. Using the electric field calculations in [13], the maximum values for the integrated electric field are then around

$$\int_{z_1}^{z_2} E_{x,y} dz = 10 \, \text{kV} \tag{12}$$

assuming an 1 A, 5 keV electron beam. Neglecting magnetic effects and scaling to HL-LHC and HEL design parameters (Table II–III) this yields a kick of:

$$\int_{z_1}^{z_2} E_x dz = 36 \, \text{kV} \Rightarrow \Delta x' = 5.1 \, \text{nrad} \tag{13}$$

Assuming now 10% fluctuation between entrance and exit kick, the expected kick from the HEL bends is

$$\Delta x', \Delta y' = 0.5 \, \text{nrad}. \tag{14}$$

B. Kicks in the central region (main solenoid)

For a perfectly uniform, annular and radially symmetric profile, the field in the region of the proton beam core vanishes (see Eqn. 2). In case of electron beam profile imperfections in particular the radial symmetry is broken, leading to a residual field at the beam core (see Fig. 4). A first estimate of the residual kick for the HEL design parameters (Table II–III) with a main solenoid field of $B_m = 5 \, \text{T}$ can be obtained by scaling the electric field at the center from the measurements and simulations shown in Fig. 4, yielding:

$$\Delta x', \Delta y' = 15 \, \text{nrad} \tag{15}$$

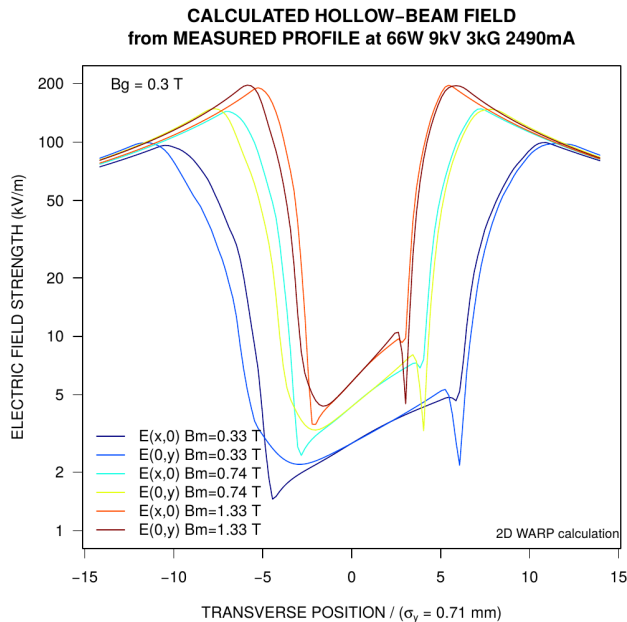New gun measurements, can we maybe have a WARP simulation for the new design parameters instead of scaling?

FIG. 4. Calculated hollow electron beam field from measured profile of 9 kV, 2.49 A e-gun and different main solenoidal fields Bm. The field has been calculated using the code WARP [17]. *change Bm to B_m +substitute with new picture.*

IV. LHC EXPERIMENTS

A. Overview of LHC experiments

The experiments at the LHC presented in this paper were aiming at deriving tolerances on the residual HEL field at the location of the beam core in case of pulsed operation. In total, two experiments were conducted, the first one in 2016 [18] and the second one in 2017 [19]. The beam and machine parameters for both experiments are summarized in Table IV. As there is currently no HEL installed in the LHC, the kick on the beam core is emulated by a dipole kick applied with the transverse damper of which more details are given in Section IV B. Explicitly, all orders higher than the first order are neglected. Preceding the beam experiments, simulations were performed to identify the most effective pulsing pattern for the kth turn pulsing (see Sec. IV D 1) and yield estimates for losses and emittance growth. The two k^{th} turn pulsing patterns with the largest effect, one k^{th} turn pulsing pattern with no effect and the random excitation could then be experimentally tested in the LHC limited obviously by the beam time available. To at least test the reproducibility of the results on the example of one pulsing pattern, the 7th turn turn pulsing was tested in the 2016 experiments and then repeated in the 2017. During the experiments the losses were measured with the fast beam current transformers (FBCT) and the emittance and transverse beam profiles with the beam synchrotron

radiation telescope (BSRT). The analysis of the BSRT profiles is quite involved and we therefore concentrate in this paper only on the main results. A detailed description of the analysis can be found in [20] and for the individual experiments in [18, 19].

B. Excitation with transverse damper and filling scheme

Daniel's part

- error on amplitude
- synchronization of H and V kicker
- random noise on amplitude - is there any?
- bandwidth - why does the damper not affect the nth turn pulsing????
- filling scheme

C. Overview of simulations

For the preparation and interpretation of the experiments two different types of simulations were performed:

1. tracking of a Gaussian distribution (Distribution Tracking) to obtain loss rates and emittance growth,

2. Frequency map analysis (FMA) [21] for the visualization of resonances.

For both simulation types, the tracking code Lifetrac [22] was used and the simulation parameters are summarized in Table V. Further details on the simulations can be found in [16, 23].

D. Simulation and experimental results

In the following we will summarize the simulation and experimental results. We will jump forth and back between both as the experimental results are best understood on the base of the simulations.

In summary, the most efficient pulsing patterns and the general tendency of the distribution changes could be successfully predicted in simulations (Sec. IV D 1). Quantitative predictions of loss rates and emittance growth though failed as both observables are influenced also by the natural noise present in the LHC like ground motion and tune modulation. At injection this natural noise component is now known for the LHC. The observed effect is then the result of the interaction of the external excitation with the natural noise present.

In case of a resonant excitation, the beam distribution adjusts to a new equilibrium distribution. In the presence of only a resonant excitation, this distribution is stable

TABLE IV. Beam parameters and machine configuration as used in the two resonant excitation experiments in 2016 and 2017 [18, 19]. The plane of the excitation is abbreviated with H for horizontal, V for vertical and H+V horizontal and vertical at the same time.

Parameter	Experiment 2017	Experiment 2016
beam	Beam 1	
beam energy	injection energy, 450 GeV	
single bunch intensity	0.7×10^{11}	
normalized emittance	$2.5 - 3.5\ \mu$m	
4σ bunch length	1.3 ns	
1σ bunch length	9.7 cm	
number of bunches	$3 \times 72 = 216$ bunches (+ 1 pilot + 12 nominal)	$12 \times 4 = 48$ single bunches
injection optics, $\beta^* = 11$ m	standard optics 2017	standard optics 2016
Landau damping octupoles	$I_{\mathrm{MO}} = \pm 19.6$ A, explicitly +19.6 A for MOF circuit and -19.6 A for MOD circuit (standard 2016 settings)	
working point (Q_x, Q_y)	(62.27,60.295)	(64.28,59.31)
chromaticity (Q'_x, Q'_y)	(+15,+15)	
pulsing patterns	7th turn H,V,H+V; 8th turn H,V,H+V; random H,V,H+V;	7th turn H; 10th turn V;

and stays unchanged. If the resonant excitation inter-acts with the natural noise sources, the beam distribution still changes to a new equilibrium distribution but this change is also accompanied by a resonant excitation amplitude dependent emittance growth. Both effects were experimentally observed in case of the 10th turn pulsing (Sec. IV D 2).

TABLE V. Summary of simulation parameters for the Distribution Tracking and FMA analysis. For details see [16, 23].

Parameter	Distribution Tracking	FMA
beam	Beam 1	
beam energy	450 GeV	
emittance	3.5 μm	2.5 μm
4σ bunch length	1.3 ns	
1σ bunch length	9.7 cm	
particle	6D Gaussian	equally spaced grid
distribution	distribution (10^4 particles)	in x,y up to 10 σ with $\frac{\Delta p}{p_0} = 0$
turns tracked	10^6 turns	10^4 turns
optics	2016 or 2017 injection optics, $\beta^* = 11$ m	
machine	standard errors	no errors
imperfections	with $a_1 = b_1 = a_2 = 0^{\mathrm{a}}$	
octupoles	$I_{\mathrm{MOF}} = +19.6$ A, $I_{\mathrm{MOD}} = -19.6$ A	
tune (Q_x, Q_y)	(64.28,59.31) for 2016, (62.27,60.295) for 2017	
chromaticity (Q'_x, Q'_y)	(+15,+15)	
transv. aperture	5.7 σ	-
long. aperture	10 σ	-

$^{\mathrm{a}}$ Orbit errors are disabled due to different implementation of the a_1, b_1 errors in Lifetrac and MAD-X. b_2 errors are adjusted to yield an average (over 60 seeds) peak β-beat of 15% as expected from optics measurements in the LHC.
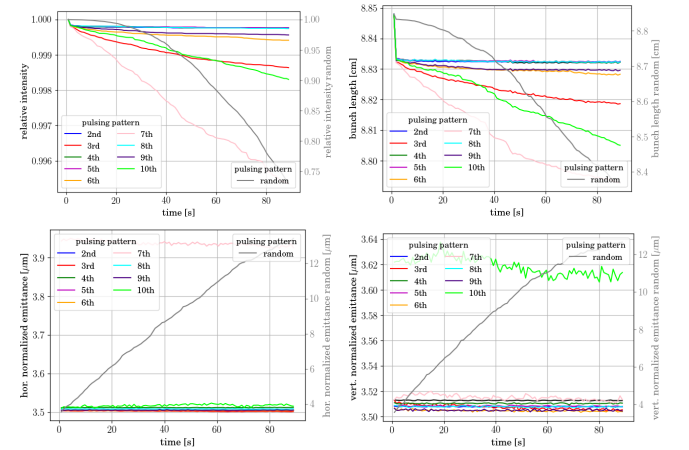
In case of an excitation with random uniform noise, the shape of the distribution does stay Gaussian. The inter-action with the natural noise source then only manifests itself in an underestimation of loss rates and emittance growth (see Sec. IV D 4). This effect was also studied in more detail in [24, 25] for colliding beams at the LHC.

1. Prediction of the most efficient pulsing pattern

In order to predict the most efficient pulsing pattern, the loss rate and emittance growth from the Distribution

FIG. 5. Relative intensity (top left), bunch length (top right) and horizontal (bottom left) and vertical (bottom right) emit-tance obtained from simulation results (Distribution Tracking) for different pulsing patterns based on the 2016 injection optics with $(Q_x, Q_y) = (64.28, 59.31)$ with standard errors. The excitation was applied in both planes with an amplitude of 96 nrad.

Tracking are compared for the different pulsing patterns. The results for the 2016 optics and tune are shown in Fig. 5. The largest losses are observed for 3rd, 7th and 10th turn pulsing and the random excitation. As the bunch length decreases accordingly, the losses are mostly associated to off-momentum particles. Only for the 7th and 10th turn pulsing as well as random excitation a considerable emittance growth is visible, where the random excitation has by far the strongest effect compared to any k^{th} turn pulsing pattern.
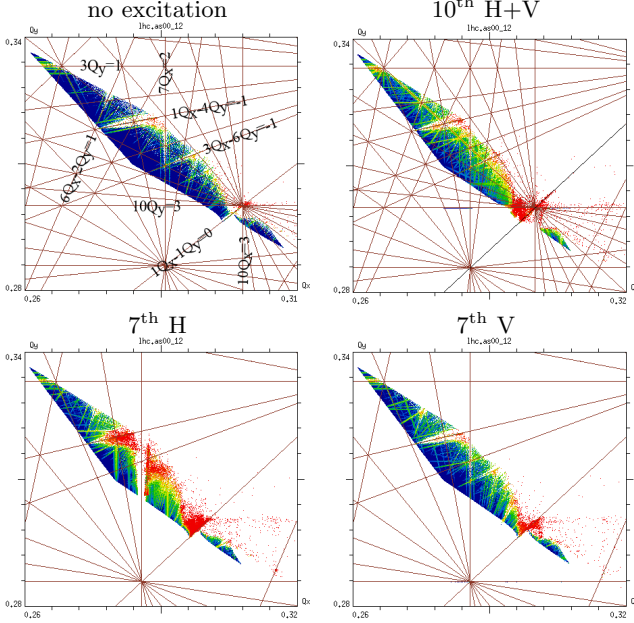
FIG. 6. FMA analysis for 7th and 10th turn pulsing based on the 2016 injection optics with no machine errors and a tune of (64.28,59.31). The excitation is 120 nrad in the corresponding plane. The absence of a strong excitation of any resonance in case of 7th turn pulsing only in V and the strong excitation in case of pulsing only in H further confirms that indeed the $7Q_x$ resonance is driven. For 10th turn pulsing there is in contrast no significant difference between pulsing only in H, only in V or in H+V.

The sensitivity to the 7th and 10th turn pulsing is also observed in absence of machine errors in which case the only source of non-linearities are the strong sextupoles and octupoles [16]. The FMA analysis shown in Fig. 6 reveals that the $7Q_x$ resonance is excited in case of the 7th turn pulsing and the $10Q_x$ and $10Q_y$ resonance in case of the 10th turn pulsing. As octupoles can only drive even resonances, the source of the $7Q_x$ resonances are the sextupoles while the octupoles only generate the tune footprint. The other pulsing patterns do not exhibit any increase in losses or emittance growth without magnetic errors and their effect thus is based on the magnetic field errors assigned, explicitly also the seed chosen for the simulations.

For the 7th and 10th turn pulsing the emittance also appears to start at an increased initial value and then stays almost constant. This behavior is due to the adjustment
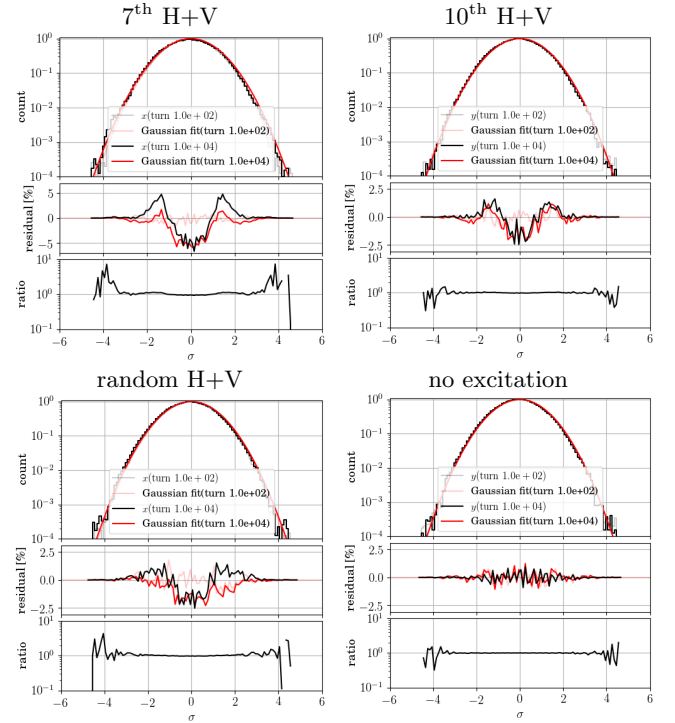

FIG. 7. Horizontal beam distribution for 7th turn (top left), vertical beam distribution for 10th turn pulsing (top right) and horizontal (bottom left) and vertical (bottom right) beam distribution for random excitation from simulation results (Distribution Tracking) based on the 2016 injection optics with $(Q_x, Q_y) = (64.28, 59.31)$ with standard errors. The excitation was applied in both planes with an amplitude of 96 nrad. The residual is defined as the final distribution (here 10^4 turns) minus the initial distribution (here 10^2 turns), and the ratio as the final distribution divided by the initial distribution. The red line in the residual shows the difference between the Gaussian fit of the distribution and the distribution itself.

of the beam distribution during the first 10^4 turns to a new equilibrium distribution. As the beam distribution is only dumped every 10^4 turns, this initial fast adjustment manifests itself in an increased initial emittance value in Fig. 5. Besides an increased emittance, the new distribution also becomes non-Gaussian as can be seen from the residual in respect to the Gaussian distribution in case of the 7th and 10th turn pulsing (Fig. 7). For comparison, also the distribution in both planes for a random excitation is shown This initial fast change of the beam distribution was also to the knowledge of the authors for the first time experimentally observed (Sec. IV D 2 and Sec. IV D 5). The timescale of this fast adjustment is experimentally however much slower than predicted in simulations - on the timescale of minutes compared to seconds.

2. 10th turn pulsing

The 10th turn pulsing was tested in 2016 with an excitation in the vertical plane only. In summary, the following experimental results were obtained:

1. increase of the loss rate with the excitation amplitude (Fig. 8, 11),

2. increase of the emittance growth with the excitation amplitude in the vertical plane but not in the horizontal plane (Fig. 8).

3. change of the beam distribution due to the resonant excitation (Fig. 8, 9)

As loss rates, emittance growth and distribution stayed unchanged for the 4 reference bunches, the above observations can be truly associated with the effect of the resonant excitation.
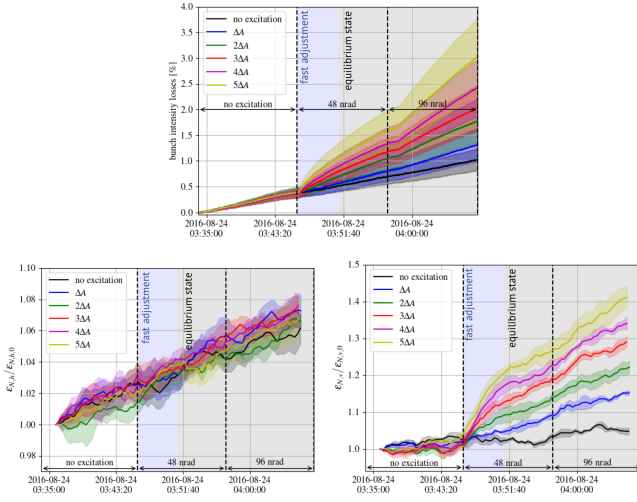
FIG. 8. Relative intensity (top) and emittance (bottom) obtained during the 2016 experiments. For each maximum amplitude A_{max} = 48 nrad and 96 nrad, the excitation amplitude was linearly increased for each group of 4 bunches (see Sec. IV B). The different colored solid lines labeled with $n\Delta A$ indicate the average over the 4 bunches with the same excitation amplitude together with the 1σ standard deviation as their envelope.

Besides the determination of the scaling of the loss rate and emittance growth with the excitation amplitude as required for the specification of the hollow electron lens, the most novel observation is the direct measurement of the change of the beam distribution, here with the Beam Synchrotron Radiation Telescope (BSRT) [20]. As an example for the change in distribution, the vertical profile of a reference bunch and one bunch experiencing the maximum excitation are compared in Fig. 9. The distribution of the excited bunch clearly changes and becomes non-Gaussian, while the reference bunch stays almost unchanged.
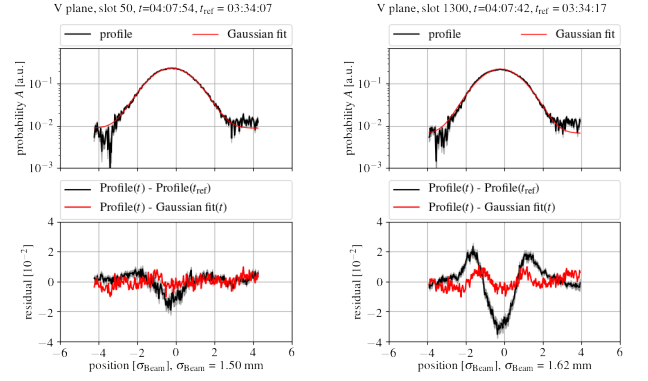
FIG. 9. Vertical beam profiles measured with the Beam Synchrotron Radiation Telescope (BSRT) during the 2016 experiments. The profiles are taken at the end of the 10th turn pulsing in V. The black line in the plot of the residual is the current profile minus the initial profile and is a measure for the overall change of the distribution. The red line is the current profile minus its Gaussian fit, which gives and indication for the deviation of the distribution from a Gaussian distribution. For details on the analysis see [20]. The distribution of the reference bunch (left), here slot 50, stays unchanged, while the bunch experiencing the maximum excitation (right), here slot 1300, clearly shows a change to a non-Gaussian distribution.

Comparing these experimental results with the simulations including only the 10th turn pulsing (solid line, Fig. 10), the simulations predict qualitatively correctly an excitation amplitude dependent loss rate, but fail to predict the excitation amplitude dependent, continuous emittance growth seen experimentally. Instead, the simu-
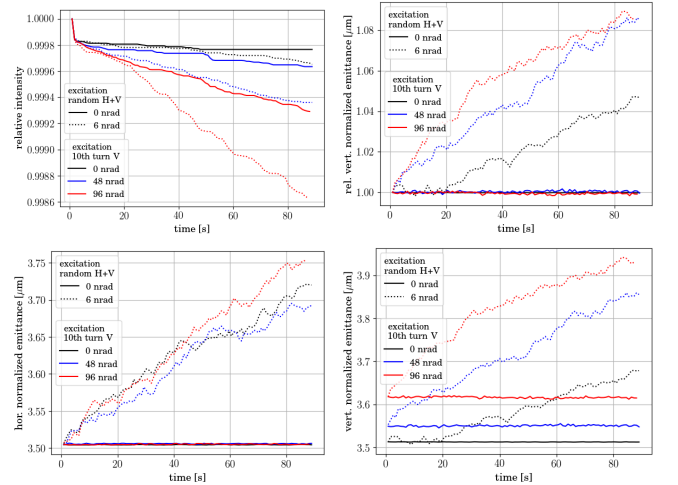
FIG. 10. Relative intensity (top left) and relative vert. emittance (top right), and hor. (bottom left) and vert. (bottom right) emittance obtained from simulations (Distribution Tracking) based on the 2016 injection optics with standard errors and $(Q_x, Q_y) = (64.28, 59.31)$. The solid line indicates an excitation with only 10th turn pulsing in V and the dotted line with 10th turn pulsing in V plus a random dipole noise component in H+V of 6 nrad.

lations yield a constant emittance after an initial increase during the first 10^4 turns or first second. So obviously there is an essential ingredient missing. As it turns out, the constant emittance can be changed to an excitation amplitude dependent emittance growth by adding a random dipole noise component with uniform distribution (dotted line in Fig. 10). As a first estimate the value obtained in [24, 25] for 6.5 TeV was used and scaled by the magnetic rigidity to the injection energy of 450 GeV, as no noise estimate is available at injection. This yields a maximum kick amplitude at the transverse damper of approximately

$$\theta_{\mathrm{random,ADT,max}}(450 \text{ GeV}) = 6 \text{ nrad}, \qquad (16)$$

Adding this random noise component, the simulations then yield correctly an excitation amplitude dependent emittance growth in the vertical plane only after a first fast adjustment of the beam distribution visible as an increased initial value.

Adding a random noise component has in addition the effect of increasing the loss rate. As the loss rates are in general underestimated in simulations compared to the experimental results, the discrepancy between simulations and experiment is therefore further reduced, but a large difference still prevails (Fig. 11).
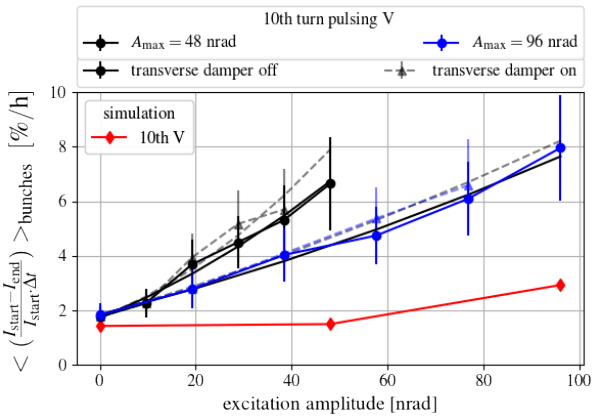

FIG. 11. Comparison of scaling of loss rates with the 10th turn pulsing excitation amplitude. The experimental results are shown in black (maximum excitation with 48 nrad) and blue (maximum excitation with 96 nrad) and the simulation results (2016 injection optics, standard errors, $(Q_x, Q_y) = (64.28, 59.31)$, 10th turn pulsing in V plus random dipole noise in H+V of 6 nrad) in red.

3. *8th turn pulsing*

4. *random excitation*

5. *7th turn pulsing*

The 7th turn pulsing pattern is the only pulsing pattern which has been tested during both experiments in 2016 and 2017 and was intended to serve as a proof for the reproducibility of the results. However, in 2017 the machine tune was changed from (64.28,59.31) to (62.27,60.295) in standard operation accompanied by a slight change in optics. The attempt to change back to the fractional tune of (.28,.31) as chosen in 2016 however lead to large losses during the experiments in 2017. This change in tune entailed a change in the driving resonances, from previously the $7Q_x$ resonances in 2016 (Fig. 6) to the $7Q_x$, $7Q_y$ and $7Q_x + 7Q_y$ resonance in 2017 (Fig. 12) and in addition also the effected amplitudes of the beam distribution. Therefore the effects on
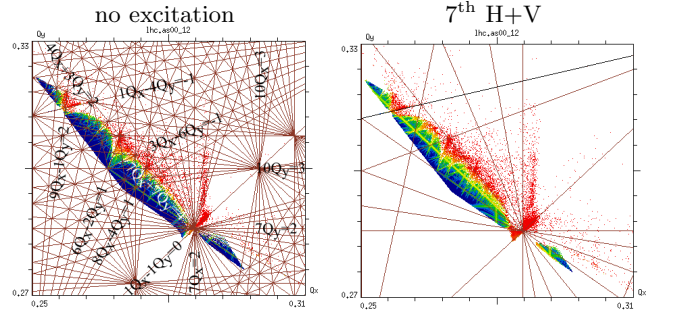

FIG. 12. FMA analysis for 7th turn pulsing based on the 2017 injection optics with no machine errors and a tune of (62.27,60.295). The excitation is 96 nrad in both planes. The $7Q_x$ and $7Q_y$ resonance are both excited and in addition the 14th order $7Q_x + 7Q_y$.

the beam also differ for both experiments (see Table VI for a general overview and Fig. **??** and Appendix **??** for more details). Simulations more or less fail completely

TABLE VI. Overview of the effect of 7th turn pulsing during the two resonant excitation experiments in 2016 and 2017 [18, 19]. The plane of the excitation is abbreviated with H for horizontal, V for vertical and H+V for horizontal and vertical at the same time.

Parameter	Experiment 2017	Experiment 2016
tune (Q_x, Q_y)	(62.27,60.295)	(64.28,59.31)
excitation plane	H,V and H+V	H
losses	similar loss rates for pulsing in H,V and H+V	losses for pulsing in H
hor. emit. growth	no	yes, very small
vert. emit. growth	yes, for pulsing in V and H+V	no

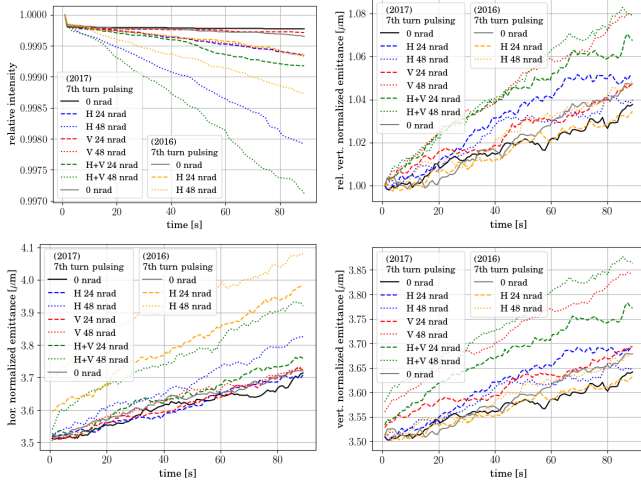(Fig. 13). Higher amplitudes have been used for simulations to see noticable effect.

FIG. 13. Relative intensity (top left) and relative vert. emittance (top right), and hor. (bottom left) and vert. (bottom right) emittance obtained from simulations (Distribution Tracking) based on the 2016 injection optics with standard errors and $(Q_x, Q_y) = (64.28, 59.31)$ and 2017 injection optics with standard errors and $(Q_x, Q_y) = (62.27, 60.295)$. The solid line indicates an excitation with only a random dipole noise component in H+V of 6 nrad, and the dotted and dashed line the results for 7th turn pulsing plus a random dipole noise component in H+V of 6 nrad.

- Don't understand why there is emittance growth in H for 2016. There is no emittance growth in the experiment.

- repeat simulations for 2017 for all three planes and with random noise =¿ check if there is only emittance growth in V done.

- experimentally: 2016 + 2017 losses in all cases, only emittance growth in V in 2017

6. Effect of the transverse damper

Compare random and nth turn -¿ no damping for nth, only for random.

In general:

- repeat simulations for each kth turn pattern with only b2 errors (done)

- show results when adding random noise -¿ amplitude dependent emittance growth + losses

- FMA plot of 7th (2017) -¿ explain why in H and in V both losses, FMA plot of 10th (2016), FMA plot of 8th and random

- beam distribution change for 10th
- 7th turn: small emittance but high losses

- 8th turn: almost no effect

- 10th turn: adjustment of distribution -¿ emittance growth + small losses

- random: constant filamentation -¿ emittance growth + later strong losses when beam hits aperature

V. SUMMARY

ACKNOWLEDGMENTS

Appendix A: Appendixes

Appendix B: Results of 7th turn pulsing during 2016 and 2017 experiments

[1] S. Holmes, R. S. Moore, and V. Shiltsev, Journal of Instrumentation **6**, T08001 (2011).

[2] D. Nisbet, "2016 operation: Operational efficiency and lessons learnt," (2017), LHC Performance Workshop 2017.

[3] O. S. Brüning, P. Collier, P. Lebrun, S. Myers, R. Ostojic, J. Poole, and P. Proudlock, *LHC Design Report*, CERN Yellow Reports: Monographs (CERN, Geneva, 2004).

[4] A. G., B. A. I., B. O., F. P., L. M., R. L., and T. L., *High-Luminosity Large Hadron Collider (HL-LHC): Technical Design Report V. 0.1*, CERN Yellow Reports: Monographs (CERN, Geneva, 2017).

[5] M. Benedikt and F. Zimmermann, *Future Circular Colliders*, Tech. Rep. CERN-ACC-2015-0164 (CERN,

Geneva, 2015).

[6] G. Valentino, "What did we learn about halo population during MDs and regular operation?" (2016), Review of the needs for a hollow e-lens for the HL-LHC.

[7] "Review on the needs for a hollow e-lens for the HL-LHC," (2016).

[8] R. Bruce, "Alternative methods for halo depletion (damper, tune modulation, and wire), long range beam-beam and comparison of their performance/reliability to that of a hollow electron lens." (2016), review of the needs for a hollow e-lens for the HL-LHC.

[9] *Proceedings, EuCARD-AccNet-EuroLumi Workshop: The High-Energy Large Hadron Collider (HE-LHC10): Villa Bighi, Malta, Republic of Malta, October 14-16, 2010* (2011) arXiv:1108.1617 [physics.acc-ph].

[10] G. Stancari, A. Valishev, G. Annala, G. Kuznetsov, V. Shiltsev, D. A. Still, and L. G. Vorobiev, Phys. Rev. Lett. **107**, 084802 (2011).

[11] X.-L. Zhang, K. Bishofberger, V. Kamerdzhiev, V. Lebedev, V. Shiltsev, R. Thurman-Keup, and A. Tollestrup, Phys. Rev. ST Accel. Beams **11**, 051002 (2008).

[12] G. Stancari, V. Previtali, A. Valishev, R. Bruce, S. Redaelli, A. Rossi, and B. S. Ferrando, *Conceptual design of hollow electron lenses for beam halo control in the Large Hadron Collider*, Tech. Rep. FERMILAB-TM-2572-APC, CERN-ACC-2014-0248 (Fermilab, CERN, 2014) arXiv:1405.2033 [physics.acc-ph].

[13] G. Stancari, *Calculation of the Transverse Kicks Generated by the Bends of a Hollow Electron Lens*, Tech. Rep. FERMILAB-FN-0972-APC (Fermilab, 2014) arXiv:1403.6370 [physics.acc-ph].

[14] I. A. Morozov, G. Stancari, A. Valishev, and D. N. Shatilov, *Proceedings, 3rd International Conference on Particle accelerator (IPAC 2012): New Orleans, USA, May 2-25, 2012*, Conf. Proc. **C1205201**, 94 (2012).

[15] "Hl-lhc optics v1.3," LHC optics web.

[16] M. Fitterer, G. Stancari, and A. Valishev, *Effect of pulsed hollow electron-lens operation on the proton beam core in LHC*, Tech. Rep. FERMILAB-TM-2635-AD (Fermilab, 2016).

[17] "The warp code,".

[18] M. Fitterer, G. Stancari, A. Valishev, R. Bruce, P. S. Papadopoulou, G. Papotti, D. Pellegrini, S. Redaelli, G. Trad, D. Valuch, G. Valentino, J. Wagner, and C. Xu, (2016).

[19] M. Fitterer, G. Stancari, A. Valishev, R. Bruce, P. S. Papadopoulou, G. Papotti, D. Pellegrini, S. Redaelli, G. Trad, D. Valuch, G. Valentino, J. Wagner, and C. Xu, (2018).

[20] M. Fitterer and G. Stancari, *Analysis of BSRT profiles in the LHC at injection*, Tech. Rep. FERMILAB-TM-2657-AD-APC (Fermilab, 2017).

[21] J. Laskar, *Particle accelerator. Proceedings, Conference, PAC 2003, Portland, USA, May 12-16, 2003*, Conf. Proc. **C030512**, 378 (2003).

[22] D. Shatilov, Y. Alexahin, V. Lebedev, and A. Valishev, *Particle accelerator. Proceedings, Conference, PAC'05,Knoxville, USA, May 16-20, 2005*, Conf. Proc. PAC'05 (2005).

[23] M. Fitterer, G. Stancari, and A. Valishev, *Update on simulations of the effect of pulsed hollow electron-lens operation on the proton beam core in LHC*, Tech. Rep. FERMILAB-TM-??-AD (Fermilab, 2018).

[24] X. Buffat, N. Biancacci, S. V. Furuseth, D. Jacquet, E. Metral, D. Pellegrini, M. Pojer, G. Trad, D. Valuch, J. Barranco Garcia, T. Pieloni, C. Tambasco, and Q. Li, (2017).

[25] J. Barranco Garcia, X. Buffat, T. Pieloni, C. Tambasco, G. Trad, D. Valuch, M. Betz, M. Wendt, M. Pojer, M. Solfaroli Camillocci, B. M. Salvachua Ferrando, K. Fuchsberger, M. Albert, and J. Qiang, *MD 400: LHC emittance growth in presence of an external source of noise during collision*, Tech. Rep. CERN-ACC-NOTE-2016-0020 (CERN, 2016).